Research Article | Vol. 9, No. 8 | 1 Aug 2018 | OPTICAL MATERIALS EXPRESS 2072
Optical Materials EXPRESS

Optical properties of refractory metal based thin films

ARCHAN BANERJEE,[1,2,*] ROBERT M. HEATH,[1] DMITRY MOROZOV,[1] DILINI HEMAKUMARA,[1] UMBERTO NASTI,[1] IAIN THAYNE,[1] AND ROBERT H. HADFIELD[1]

[1]*School of Engineering, University of Glasgow, Glasgow G12 8QQ, UK*
[2]*Presently at: Centre for Quantum Photonics, University of Bristol, Bristol BS8 1TH, UK*
**a.banerjee@bristol.ac.uk*

Abstract There is growing interest in refractory metal thin films for a range of emerging nanophotonic applications, including high temperature plasmonic structures and infrared superconducting single photon detectors. We present a detailed comparison of optical properties for key representative materials in this class (NbN, NbTiN, TiN and MoSi) with texture varying from crystalline to amorphous. NbN, NbTiN and MoSi have been grown in an ultra-high vacuum sputter deposition system on silicon substrates at room temperature. Two different techniques (sputtering and atomic layer deposition) have been employed to deposit TiN. We have carried out variable angle ellipsometric measurements of optical properties from ultraviolet to mid-infrared wavelengths. We compare with high resolution transmission electron microscopy analysis of microstructure. Sputter-deposited TiN and MoSi have shown the highest optical absorption in the infrared wavelengths relative to NbN, NbTiN and ALD-deposited TiN. We have also modelled the performance of a semi-infinite metal air interface as a plasmonic structure with the above mentioned refractory metal based thin films as the plasmonic components. This study has implications for the design of next-generation superconducting nanowire single photon detectors and plasmonic nanostructure-based devices.

OCIS codes: (160.4670) Optical materials; (310.6860) Thin films, optical properties; (120.4530) Optical constants; (250.5403) Plasmonics; (040.3060) Infrared detectors.

References and links

1. T. E. Tietz and J. W. Wilson, *Behavior and Properties of Refractory Metals* (Stanford University Press, 1965).
2. M. Bauccio, *ASM Metals Reference Book* (ASM International, 1993).
3. E. Lassner and W.-D. Schubert, *Tungsten : Properties, Chemistry, Technology of the Element, Alloys, and Chemical Compounds* (Kluwer Academic/Plenum Publishers, 1999).
4. D. Cristea, I. Ghiuță, and D. Munteanu, "Tantalum based materials for implants and prosthesis applications," Bull. Transilv. Univ. Brașov **857**(2), (2015).
5. M. E. Packer and M. J. Murray, "A floating zone furnace for melting refractory metals and metal-like compounds," J. Phys. Educ. **5**(3), 246 (1972).
6. R. E. Smallwood, ASTM Committee B-10 on Reactive and Refractory Metals and Alloys, and L. Symposium on Refractory Metals and Their Industrial Applications, *Refractory Metals and Their Industrial Applications: A Symposium* (ASTM, 1984).
7. A. Boltasseva and H. A. Atwater, "Materials science. Low-loss plasmonic metamaterials," Science **331**(6015), 290–291 (2011).
8. A. Banerjee, L. J. Baker, A. Doye, M. Nord, R. M. Heath, K. Erotokritou, D. Bosworth, Z. H. Barber, I. MacLaren, and R. H. Hadfield, "Characterisation of amorphous molybdenum silicide (MoSi) superconducting thin films and nanowires," Supercond. Sci. Technol. **30**(8), 084010 (2017).
9. A. E. Lita, V. B. Verma, R. D. Horansky, J. M. Shainline, R. P. Mirin, and S. Nam, "Materials Development for High Efficiency Superconducting Nanowire Single-Photon Detectors," MRS Proc. **1807**, 1–6 (2015).
10. D. Bosworth, S.-L. Sahonta, R. H. Hadfield, and Z. H. Barber, "Amorphous molybdenum silicon superconducting thin films," AIP Adv. **5**(8), 087106 (2015).
11. D. M. O'Carroll, "Nanophotonics and plasmonics for solar energy harvesting and conversion," J. Photonics Energy **5**(1), 057001 (2015).

#326346 https://doi.org/10.1364/OME.8.002072
Journal © 2018 Received 23 Mar 2018; revised 19 May 2018; accepted 21 Jun 2018; published 5 Jul 2018

Optical Materials EXPRESS

12. J. N. Anker, W. P. Hall, O. Lyandres, N. C. Shah, J. Zhao, and R. P. Van Duyne, "Biosensing with plasmonic nanosensors," Nat. Mater. **7**(6), 442–453 (2008).
13. A. Lalisse, G. Tessier, J. Plain, and G. Baffou, "Plasmonic efficiencies of nanoparticles made of metal nitrides (TiN, ZrN) compared with gold," Sci. Rep. **6**(1), 38647 (2016).
14. P. Patsalas, N. Kalfagiannis, and S. Kassavetis, "Optical properties and plasmonic performance of titanium nitride," Materials (Basel) **8**(12), 3128–3154 (2015).
15. W. Li, U. Guler, N. Kinsey, G. V. Naik, A. Boltasseva, J. Guan, V. M. Shalaev, and A. V. Kildishev, "Refractory plasmonics with titanium nitride: broadband metamaterial absorber," Adv. Mater. **26**(47), 7959–7965 (2014).
16. J. A. Briggs, G. V. Naik, Y. Zhao, T. A. Petach, K. Sahasrabuddhe, D. Goldhaber-Gordon, N. A. Melosh, and J. A. Dionne, "Temperature-dependent optical properties of titanium nitride," Appl. Phys. Lett. **110**(10), 101901 (2017).
17. J. Chen, J. B. Altepeter, M. Medic, K. F. Lee, B. Gokden, R. H. Hadfield, S. W. Nam, and P. Kumar, "Demonstration of a quantum controlled-NOT gate in the telecommunications band," Phys. Rev. Lett. **100**(13), 133603 (2008).
18. R. H. Hadfield, M. J. Stevens, R. P. Mirin, and S. W. Nam, "Single-photon source characterization with twin infrared-sensitive superconducting single-photon detectors," J. Appl. Phys. **101**(10), 103104 (2007).
19. J. Zhang, N. Boiadjieva, G. Chulkova, H. Deslandes, G. N. Gol'tsman, A. Korneev, P. Kouminov, M. Leibowitz, W. Lo, R. Malinsky, O. Okunev, A. Pearlman, W. Slysz, K. Smirnov, C. Tsao, A. Verevkin, B. Voronov, K. Wilsher, and R. Sobolewski, "Noninvasive CMOS circuit testing with NbN superconducting single-photon detectors," Electron. Lett. **39**(14), 1086 (2003).
20. C. M. Natarajan, M. G. Tanner, and R. H. Hadfield, "Superconducting nanowire single-photon detectors: physics and applications," Supercond. Sci. Technol. **25**(6), 063001 (2012).
21. G. N. Gol'tsman, O. Okunev, G. Chulkova, A. Lipatov, A. Semenov, K. Smirnov, B. Voronov, A. Dzardanov, C. Williams, and R. Sobolewski, "Picosecond superconducting single-photon optical detector," Appl. Phys. Lett. **79**(6), 705–707 (2001).
22. S. Miki, T. Yamashita, H. Terai, and Z. Wang, "High performance fiber-coupled NbTiN superconducting nanowire single photon detectors with Gifford-McMahon cryocooler," Opt. Express **21**(8), 10208–10214 (2013).
23. F. Marsili, D. Bitauld, A. Fiore, A. Gaggero, F. Mattioli, R. Leoni, M. Benkahoul, and F. Lévy, "High efficiency NbN nanowire superconducting single photon detectors fabricated on MgO substrates from a low temperature process," Opt. Express **16**(5), 3191–3196 (2008).
24. J. Bardeen, L. N. Cooper, and J. R. Schrieffer, "Theory of superconductivity," Phys. Rev. **108**(5), 1175–1204 (1957).
25. M. S. Allman, V. B. Verma, M. Stevens, T. Gerrits, R. D. Horansky, E. Lita, F. Marsili, A. Beyer, M. D. Shaw, D. Kumor, R. Mirin, and S. W. Nam, "A near-infrared 64-pixel superconducting nanowire single photon detector array with integrated multiplexed readout," Appl. Phys. Lett. **106**(19), 192601 (2015).
26. J. Li, R. A. Kirkwood, L. J. Baker, D. Bosworth, K. Erotokritou, A. Banerjee, R. M. Heath, C. M. Natarajan, Z. H. Barber, M. Sorel, and R. H. Hadfield, "Nano-optical single-photon response mapping of waveguide integrated molybdenum silicide (MoSi) superconducting nanowires," Opt. Express **24**(13), 13931–13938 (2016).
27. R. M. Heath, M. G. Tanner, T. D. Drysdale, S. Miki, V. Giannini, S. A. Maier, and R. H. Hadfield, "Nanoantenna enhancement for telecom-wavelength superconducting single photon detectors," Nano Lett. **15**(2), 819–822 (2015).
28. W. M. Haynes, *CRC Handbook of Chemistry and Physics : A Ready-Reference Book of Chemical and Physical Data*, 92nd ed. (CRC Press, 2011).
29. M. E. Straumanis and S. Zyszczynski, "Lattice parameters, thermal expansion coefficients and densities of Nb, and of solid solutions Nb–O and Nb–N–O and their defect structure," J. Appl. Cryst. **3**(1), 1–6 (1970).
30. C. M. Perlov and C. Y. Fong, "Calculation of the superconducting transition temperature in niobium," Phys. Rev. B **29**(3), 1243–1249 (1984).
31. P. Ettmayer, R. Kieffer, and F. Hattinger, "Determination of melting points of metal nitrides under nitrogen pressure," Metall **28**(12), 1151–1156 (1974).
32. G. Zou, M. Jain, H. Zhou, H. Luo, S. A. Baily, L. Civale, E. Bauer, T. M. McCleskey, A. K. Burrell, and Q. Jia, "Ultrathin epitaxial superconducting niobium nitride films grown by a chemical solution technique," Chem. Commun. (Camb.) **44**(45), 6022–6024 (2008).
33. R. G. Ross and W. Hume-Rothery, "High temperature X-ray metallography: I. A new debye-scherrer camera for use at very high temperatures II. A new parafocusing camera III. Applications to the study of chromium, hafnium, molybdenum, rhodium, ruthenium and tungsten," J. Less Common Met. **5**(3), 258–270 (1963).
34. I. G. D 'yakov and A. D. Shvets, "Investigation of superconducting properties of molybdenum," Sov. Phys. **22**(49), 1091–1093 (1966).
35. A. Misra, J. J. Petrovic, and T. E. Mitchell, "Microstructures and mechanical properties of a Mo_3Si-Mo_5Si_3 composite," Scr. Mater. **40**(2), 191–196 (1998).
36. R. R. Pawar and V. T. Deshpande, "The anisotropy of the thermal expansion of α-titanium," Acta Crystallogr. A **24**(2), 316–317 (1968).
37. M. C. Steele and R. A. Hein, "Superconductivity of Titanium," Phys. Rev. **92**(2), 243–247 (1953).
38. H. O. Pierson, *Handbook of Refractory Carbides and Nitrides : Properties, Characteristics, Processing, and Applications* (Noyes Publications, 1996).

Optical Materials EXPRESS

39. M. Marlo and V. Milman, "Density-functional study of bulk and surface properties of titanium nitride using different exchange-correlation functionals," Phys. Rev. B **62**(4), 2899–2907 (2000).
40. W. Spengler, R. Kaiser, A. N. Christensen, and G. Müller-Vogt, "Raman scattering, superconductivity, and phonon density of states of stoichiometric and nonstoichiometric TiN," Phys. Rev. B **17**(3), 1095–1101 (1978).
41. A. Banerjee, "Optimisation of superconducting thin film growth for next generation superconducting detector applications," University of Glasgow (2017).
42. O. Madelung, U. Rössler, and M. Schulz, eds., "Silicon (Si), lattice parameter, thermal expansion," in *Group IV Elements, IV–IV and III–V Compounds. Part B - Electronic, Transport, Optical and Other Properties* (Springer Berlin Heidelberg, 2002), pp. 1–17.
43. J. N. Hilfiker, N. Singh, T. Tiwald, D. Convey, S. M. Smith, J. H. Baker, and H. G. Tompkins, "Survey of methods to characterize thin absorbing films with spectroscopic ellipsometry," Thin Solid Films **516**(22), 7979–7989 (2008).
44. Y. P. Korneeva, M. Y. Mikhailov, Y. P. Pershin, N. N. Manova, A. V. Divochiy, Y. B. Vakhtomin, A. A. Korneev, K. V. Smirnov, A. G. Sivakov, A. Y. Devizenko, and G. N. Goltsman, "Superconducting single-photon detector made of MoSi film," Supercond. Sci. Technol. **27**(9), 095012 (2014).
45. V. Anant, "Engineering the optical properties of subwavelength devices and materials," Massachusetts Institute of Technology (2007).
46. M. Leskela and M. Ritalä, "Atomic layer deposition (ALD) : from precursors to thin film structures," Thin Solid Films **409**(1), 138–146 (2002).
47. E. Alfonso, J. Olaya, and G. Cubillos, "Thin film growth through sputtering technique and its applications," in *Crystallization - Science and Technology* (InTech, 2012).
48. S. A. Maier, *Plasmonics : Fundamentals and Applications* (Springer, 2007).
49. C. Della Giovampaola and N. Engheta, "Plasmonics without negative dielectrics," Phys. Rev. B **93**(19), 195152 (2016).
50. P. Patsalas, N. Kalfagiannis, S. Kassavetis, G. Abadias, D. V. Bellas, C. Lekka, and E. Lidorikis, "Conductive nitrides: growth principles, optical and electronic properties, and their perspectives in photonics and plasmonics," Mater. Sci. Eng. Rep. **123**, 1–55 (2018).
51. H. Van Bui, A. Y. Kovalgin, and R. A. M. Wolters, "On the difference between optically and electrically determined resistivity of ultra-thin titanium nitride films," Appl. Surf. Sci. **269**, 45–49 (2013).
52. C. M. Zgrabik and E. L. Hu, "Optimization of sputtered titanium nitride as a tunable metal for plasmonic applications," Opt. Mater. Express **5**(12), 2786 (2015).
53. D. Shah, H. Reddy, N. Kinsey, V. M. Shalaev, and A. Boltasseva, "Optical properties of plasmonic ultrathin TiN Films," Adv. Opt. Mater. **5**(13), 1700065 (2017).
54. Y. Gutiérrez, R. A. de la Osa, D. Ortiz, J. Saiz, F. González, and F. Moreno, "Plasmonics in the ultraviolet with aluminum, gallium, magnesium and rhodium," Appl. Sci. **8**(2), 64 (2018).

1. Introduction

Refractory metals, their compounds and alloys represent a unique class of materials which have exceptionally high melting points (> 2000 °C), relatively high density, high hardness and show resistance toward atmospheric corrosion and deformation [1,2]. Due to their distinctive features refractory metals (RM) and metal-based compounds or alloys have many industrial applications (e.g. wire filaments [3], surgical implants [4], high temperature furnace equipment [5] etc.) [6]. In recent studies, refractory-metal-based nitrides and alloys have been found to be an attractive choice for plasmonic nanostructures [7] or superconducting nanowire based single photon detectors (SSPD/SNSPD) [8–10]. Due to their unique capability to control electromagnetic wave propagation, plasmonic device-based nanophotonic structures have applications in future generations of optical technology including novel solar energy harvesting [11], plasmonic sensors [12], and negative refractive index materials [7]. Conventional materials which have been used for the fabrication of plasmonic devices (e.g. noble metals like gold and silver) suffer from the crucial disadvantages of lower melting points and lack of durability [13]. RM-based nitrides are a promising alternative for this purpose due to their comparatively higher melting points [14–16]. In tandem SNSPDs have been emerged as a promising technology for advanced photon counting applications in the near infrared wavelengths (including quantum computing [17], characterization of quantum emitters [18], integrated circuit testing [19] etc.) [20]. RM nitrides and metal-based alloys have been widely used as the base materials for SNSPDs [8]. Apart from having optimum superconducting properties for device fabrication these materials also show high degree of structural stability even after frequent thermal cycling between room temperature and cryogenic temperatures.

Optical Materials EXPRESS

As shown in the Table 1, the melting points of refractory metals or refractory metal-based alloys or compounds are greater than 2000 °C (with the exception of Ti which has slightly lower melting point, but it has been included in the wider definition of refractory metals due to its resistance to atmospheric degradation [1]). The structural properties of these materials vary from amorphous to polycrystalline. An NbN thin film-based device was used to demonstrate the initial concept of SNSPD by Gol'tsman *et al.* [21]. Since then, NbN and NbTiN (a polycrystalline material with similar superconducting properties to NbN) have been widely used as the base material for SNSPD devices [22,23]. As shown in Table 1, NbN has the advantage of having a comparatively higher superconducting transition temperature (17 K for bulk). Hence, it is possible to fabricate NbN thin film-based devices (~5 nm or 6 nm thick) which will superconduct at 4 K. Due to the working principle of SNSPDs, ultrathin (thickness <10 nm) films are required for high efficiency single photon detector operation. Over the last 5 years, several amorphous refractory metal-based alloys (MoSi, MoGe and WSi) have emerged as promising alternative base materials for superconducting detectors [8]. Due to the amorphous nature of these materials, they allow more flexibility in the choice of substrates in comparison to NbN or NbTiN. These materials also have lower superconducting gap energies which give higher intrinsic single photon detection efficiency at longer wavelengths. Lower superconducting gap energy corresponds to the disadvantage of lower superconducting transition temperature [24]. As reported in [8], among all the refractory metal based superconducting binary alloys, molybdenum silicide (MoSi) has the unique combination of T_c > 4 K even in thin film form and a relatively low superconducting gap energy. Hence, MoSi can be a suitable amorphous material for superconducting detectors which can be operated at a temperature >2 K, avoiding the expensive cryogenics needed for <2 K operation. A crucial disadvantage of SNSPDs made with conventional materials (NbN or NbTiN) is that is that their sensitivity rapidly drops at wavelengths longer than 2μm. Superconducting material with lower energy gap (i.e. lower bulk T_c) can be explored to overcome this spectral limitation and extend the spectral range of SNSPDs into mid-infrared. TiN could be an appropriate material for this purpose.

One of the key challenges in optimizing the performance parameters of SNSPDs is to enhance the optical absorption of the device. Several approaches have been explored for this purpose, e.g. integration of the device inside an optical cavity or waveguide circuit or deposition of an anti-reflection coating on top of the device such as detectors fabricated on the top of distributed Bragg reflectors or gold mirrors [25,26]. Measurement of optical constants is crucial to simulate the optical absorption of the materials and design of advanced optical structures. In [27], Heath *et al.* showed that optical absorption in SNSPD devices can be enhanced with the help of plasmonic resonance induced by nanoantennas. This approach suffers from the shortcoming of involving a complicated multi-step fabrication process which adversely affects the device yield since different materials have been used to fabricate superconducting detectors and nanoantennas. If a single material could be used for both the SNSPD and the plasmonic structures it could be possible to fabricate the superconducting nanowire and plasmonic structures in a single fabrication step, dramatically reducing fabrication complexity. Thus, investigation of plasmonic properties in superconducting materials is a timely topic of some interest. This work will pave the way for more readily fabricated SNSPD devices with integrated plasmonic nanostructures to be engineered.

Optical Materials EXPRESS

Table 1. Comparison of melting points and superconducting properties of refractory metals or metal-based alloys or compounds

Material	Melting Point (°C)	Crystalline Structure	Lattice Parameter (Å)	Bulk Superconducting Transition Temperature, T_c (K)
Nb	2472 [28]	Crystalline (body-centred cubic)	3.30 [29]	9.1 [30]
NbN[a]	2573 [31]	Crystalline/Poly-crystalline (cF_8: 2 interpenetrating face-centred cubic lattices)	4.39 [32]	16 [23]
Mo	2623 [28]	Crystalline (body-centred cubic)	3.15 [33]	0.9 [34]
MoSi[b]	2025 [35]	Amorphous		7.5 [8]
Ti	1668 [28]	Crystalline (hexagonal close packed)	2.95 [36]	0.5 [37]
TiN[c]	2930 [38]	Crystalline (cF_8: 2 interpenetrating face-centred cubic lattices)	4.24 [39]	6 [40]

stoichiometry: a. Nb:N 1:1; b..Mo:Si 3:1; c. Ti:N 1.1

This paper focuses on the optical and plasmonic properties of a specific selection of refractory-based thin film materials (NbN, NbTiN, TiN and MoSi) which potentially may be used for superconducting detector or plasmonic based device fabrication.

2. Film growth and characterization

Thin films were grown on silicon substrates using a load-locked ultrahigh vacuum sputter deposition system (manufactured by Plassys Bestek; base pressure $< 5 \times 10^{-9}$ Torr) and an atomic layer deposition system (manufactured by Oxford Instruments Plasma Technology, integrated into a bespoke cluster tool configuration). NbN, NbTiN and TiN were grown by DC reactive sputtering in N_2/Ar environment. The target power supply was controlled in constant current mode. MoSi thin films was co-sputtered from Mo and Si targets in an argon plasma environment. The molybdenum target was sputtered using a DC power supply in constant current mode and the silicon target with an impedance matched radio frequency (RF) power supply. We grew TiN thin films in an atomic layer deposition system using TDMAT (tetrakis dimethylamino titanium, $Ti(N(CH_3)_2)_4$) as the precursor and H_2/N_2 plasma as reactive gas. The deposition process for all the RM-based thin film materials has been optimized in terms of superconducting properties for SNSPD device fabrication. The detailed description of film growth optimization has been reported in [8,41]. All the sputtered films were grown at room temperature whereas the ALD growth process was executed at 350 °C.

Optical Materials EXPRESS

Table 2. Deposition parameters used for film growth in the sputter system

	Current and Power Supplied at the targets	Gas Flow	Chamber Pressure
NbN	Nb:0.9 A	Ar:18 Sccm; N_2: 5 Sccm	0.14 Pa
NbTiN	Nb:0.9A; Ti: 0.450A	Ar:18 Sccm; N_2: 5 Sccm	0.14 Pa
MoSi	Mo: 0.3 A; Si: 125 W	Ar: 30 Sccm	0.2 Pa
TiN	Ti:0.6 A	Ar: 18 Sccm	0.18 Pa

Optical properties of refractory metal thin films are strongly correlated to the substrate which have used been for film deposition. We chose silicon as the substrate because in spite of being a lattice mismatched substrate for refractory metal nitrides (lattice parameter of silicon is 0.543 nm [42] whereas NbN has a lattice parameter of 0.439 nm [32]) silicon provides a platform for standard fabrication technology. Hence, thin films grown on silicon substrates are an attractive choice for combining superconducting detectors with waveguide circuits or optical cavities and plasmonic devices with quantum photonic circuits.

Complex refractive index measurement was carried out at room temperature using a J.A. Woollam & Co. variable angle spectroscopic ellipsometry (VASE) instrument. The spectral range of the VASE measurement is from 270 nm to 2200 nm with a wavelength resolution of 10 nm. Since all the thin film materials under consideration in this study are optically absorbing over the whole measurement range it is difficult to find a unique solution for both the film thickness and optical parameters due to strong correlations between them. To solve this problem, a 400 nm thick layer of SiO_2 was grown using plasma enhanced chemical vapor deposition (PECVD) on the top of the silicon substrate before the deposition of thin films. This optically-transparent layer of SiO_2 underneath the films helps to break the correlation between the film thickness and optical constants by interference enhancement during the VASE measurement. According to the principle of the interference enhancement method, this transparent SiO_2 under the films will generate damped interference oscillation patterns. Variation in the incident angles during data acquisition will lead to change in the modulation of interference patterns and will help to break the parameter correlation [43].

Structural properties of the thin film samples have been characterized via high resolution transmission electron microscopy (HRTEM). A JEOL ARM200cF and FEI Tecnai T20 microscope have been used for this purpose. Before the HRTEM analysis, electron transparent cross sections have been prepared using a dual beam focused ion beam (FIB) system.

3. Results

Figure 1 presents the optical constants evaluated from 5 nm thick amorphous MoSi films and its comparison with VASE measurements carried out on 5 nm thick polycrystalline NbN & NbTiN thin films deposited in the same deposition system. All the films were grown at room temperature. Film thickness has been estimated from the deposition rate and later verified with the help of transmission electron microscopy images. For NbN or NbTiN films HRTEM images show 10% higher value of thickness i.e ~5.5 nm [41]. As discussed in [8,44], MoSi thin films have very poor oxidation resistance. Therefore, during the SNSPD device fabrication process, environmental contact may degrade the quality of the films by surface oxidation. To prevent this, a protective silicon capping layer (~4 nm thick) may be deposited on the top of MoSi film in the same deposition chamber without breaking the vacuum.

Optical Materials EXPRESS

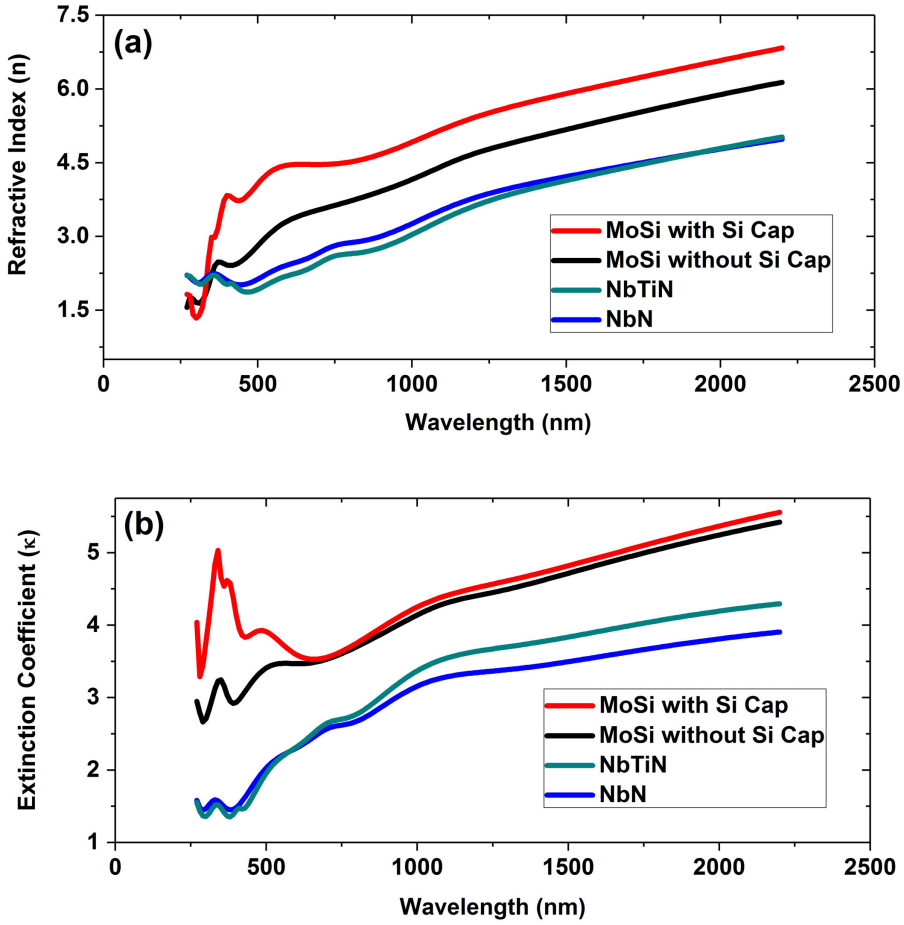

Fig. 1. Complex refractive index measurement for uncapped and capped MoSi films using variable angle spectroscopic ellipsometry (VASE) and comparison with optical constants (index of refraction *n* and extinction coefficient *κ*) measurements of NbN and NbTiN films (a) refractive index measurement of MoSi film with Si cap, MoSi film without a Si cap, NbN film and NbTiN film; (b) extinction coefficient measurement of MoSi film with Si cap, MoSi film without a Si cap, NbN film and NbTiN film.

It can be clearly seen from Fig. 1 that NbTiN film has a higher extinction coefficient (~10% higher at 1550 nm) than that of NbN film. This small enhancement in optical absorption may be explained by the presence of Ti in the lattice structure. In a previous study, Anant *et al.* reported optical constants of 12 nm thick NbN film at some specific wavelengths [45]. Their measured values of refractive index (*n*) and extinction coefficient (*κ*) at 1550 nm were n = 5.23 and κ = 5.82, which is ~1.5 times higher than our measured value (n = 4.22 and κ = 3.50). This higher value might be due to thicker films used for VASE measurements in that study.

Figure 1 also shows that MoSi films have a much higher extinction coefficient in comparison to NbN or NbTiN over the whole spectral range, which means that at any specific wavelength (*λ*) the MoSi thin films are more favorable in terms of optical absorption. We can also see that the *κ(λ)* curve of MoSi shows a continuous sharp increase even in the higher wavelength region (1500nm –2200nm). In contrast NbN or NbTiN, *κ(λ)* shows a very slow increase in that wavelength region.

Optical Materials EXPRESS

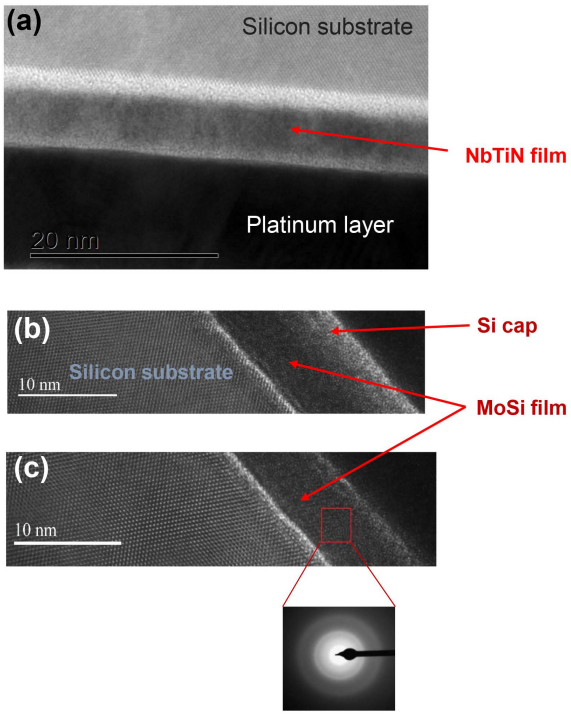

Fig. 2. High resolution transmission electron microscopy (HRTEM) analysis of NbTiN and MoSi thin films (a) TEM image of 5 nm thick NbTiN, the image shows the existence of polycrystalline structures and large grains in the film; (b) 5 nm thick MoSi with a Si cap, since the Si cap has been deposited without breaking the vacuum of the deposition system there is no sharp interface between MoSi thin film and silicon cap; (c) 5 nm thick MoSi without any Si cap (diffraction pattern recorded from the sample has been shown at the bottom of the figure) indicating the amorphous nature of the film.

As shown in previous reports, the properties of RM thin films are strongly linked to their atomic structure. Figure 2 shows HRTEM images taken from the cross-section of MoSi and NbTiN thin films samples grown on silicon substrates. Both the images demonstrate smooth and sharp film/substrate interface. Figure 2(a) confirms the polycrystalline structure of the NbTiN with columnar grains. On the other hand, Fig. 2 (b) clearly demonstrates the amorphous nature of MoSi thin films. Diffraction ring recorded from the MoSi thin film sample in the transmission electron microscope indicates the existence of structural disorder in the long range atomic scale i.e. amorphous nature of the films. In our previous study of MoSi [8], we used advanced HRTEM analysis to show that even in amorphous MoSi, there is nano crystalline structure in short (up to 1 nm) and medium range (~1- 3 nm) length scales which is similar to an A15 Mo_3Si structure.

Optical Materials EXPRESS

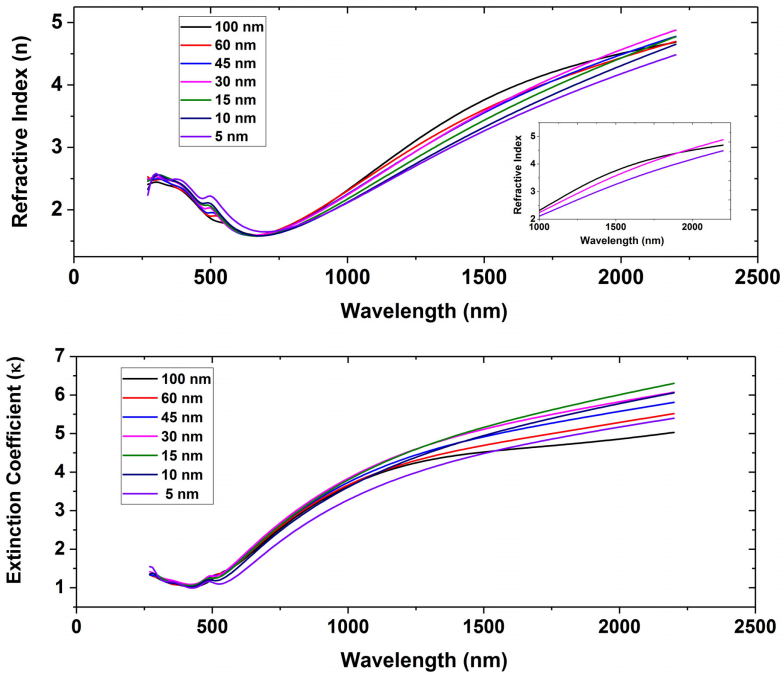

Fig. 3. Evaluation of complex refractive index of TiN thin films grown in the sputter deposition system (In the inset of top figure, a magnified view of *n(λ)* curve for 5 nm, 30 nm and 100 nm thick TiN films).

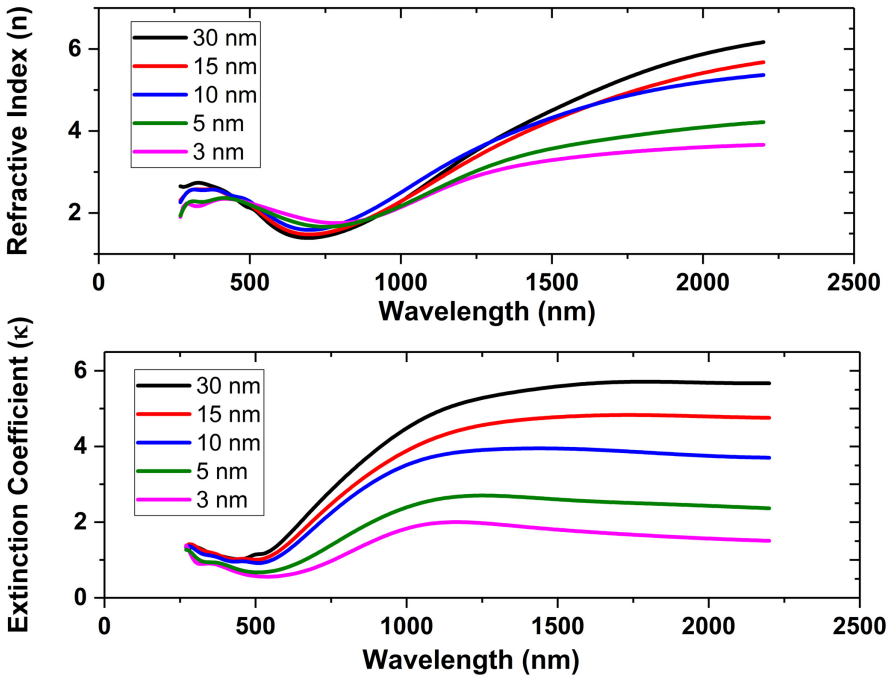

Fig. 4. Measurement of complex refractive index of TiN thin films grown in the atomic layer deposition system: extinction coefficient falls consistently with film thickness, thinnest film (3 nm thick) shows lowest value of κ over whole wavelength range.

Optical Materials EXPRESS

As mentioned in Section 2, we grew TiN thin films using two different techniques (sputtering and atomic layer deposition). Figure 3 shows the variation of complex refractive index of TiN thin films grown in the sputter deposition system as a function of wavelength. Figure 4 presents a comparison of the optical constants of TiN thin films deposited in ALD. For the sputtered TiN films (Fig. 3), there is a small variation in the extinction coefficient with film thickness (at 1040 nm it varies from 3.44 to 3.97 whereas at 2000 nm the variation spans from 4.85 to 6). This variation is not consistent with the film thickness. In the case of ALD deposited TiN films (Fig. 4), $\kappa(\lambda)$ falls consistently with film thickness (at 2000 nm wavelength, the 30 nm thick film shows a κ value of 5.68 whereas the 3 nm thick film possesses a κ value of 1.56). This deceasing trend becomes more prominent in the wavelength region 1400 nm to 2200 nm.

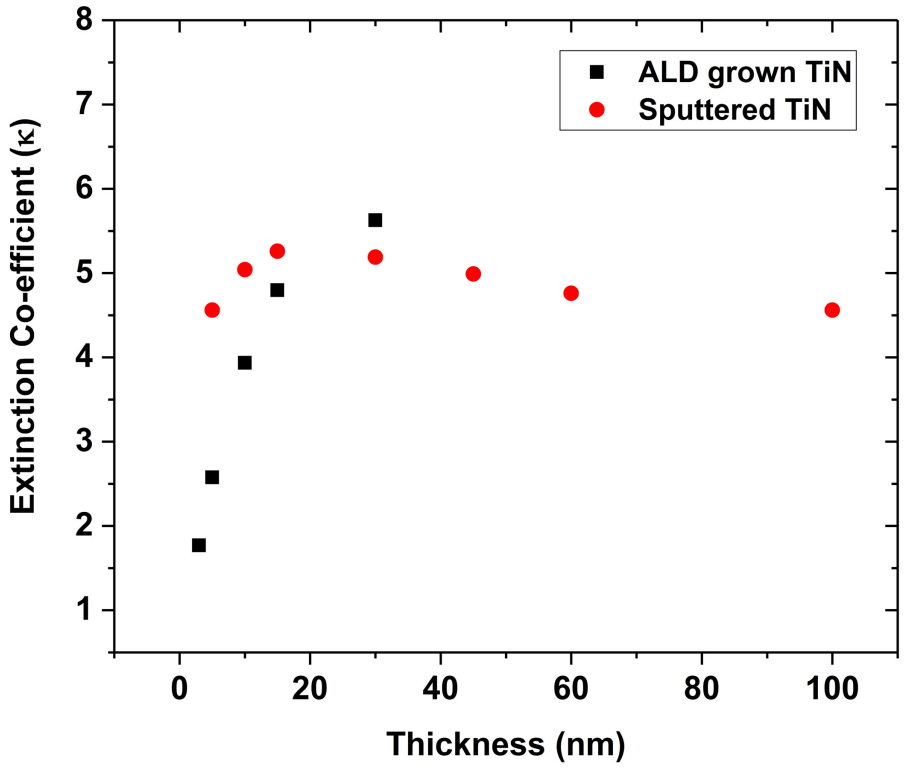

Fig. 5. Extinction coefficient (κ) for TiN films grown in two different deposition techniques (sputtering and atomic layer deposition) as a function of film thickness at 1550 nm wavelength.

Figure 5 shows how the extinction coefficient of TiN films grown in the sputter system and the ALD cluster tool varies with film thickness at 1550 nm wavelength. It is evident that TiN films deposited by the two different methods show distinct trends in how optical properties change with film thickness. This can be explained by considering differences in the underlying physical mechanism of two film deposition processes employed in this study. This difference in turn influences structural and stoichiometric properties of the films. The atomic layer deposition process is controlled by the self-limiting chemical reactions on the surface of the substrates [46]. Due to the slow deposition rate (for the film growth recipe we have used, deposition rate is 0.125 nm/minute) this process is very uniform in comparison to other film

Optical Materials EXPRESS

deposition techniques. Conversely, sputtering is a physical vapour deposition based technique where collision of charged plasma ions with the target leads to material deposition [47]. Composition of the films can easily be tuned by controlling gas flows in the chamber. In Fig. 6, we have shown HRTEM image of the TiN films indicating the crystalline texture of the films (with the existence large grains) grown in both the techniques.

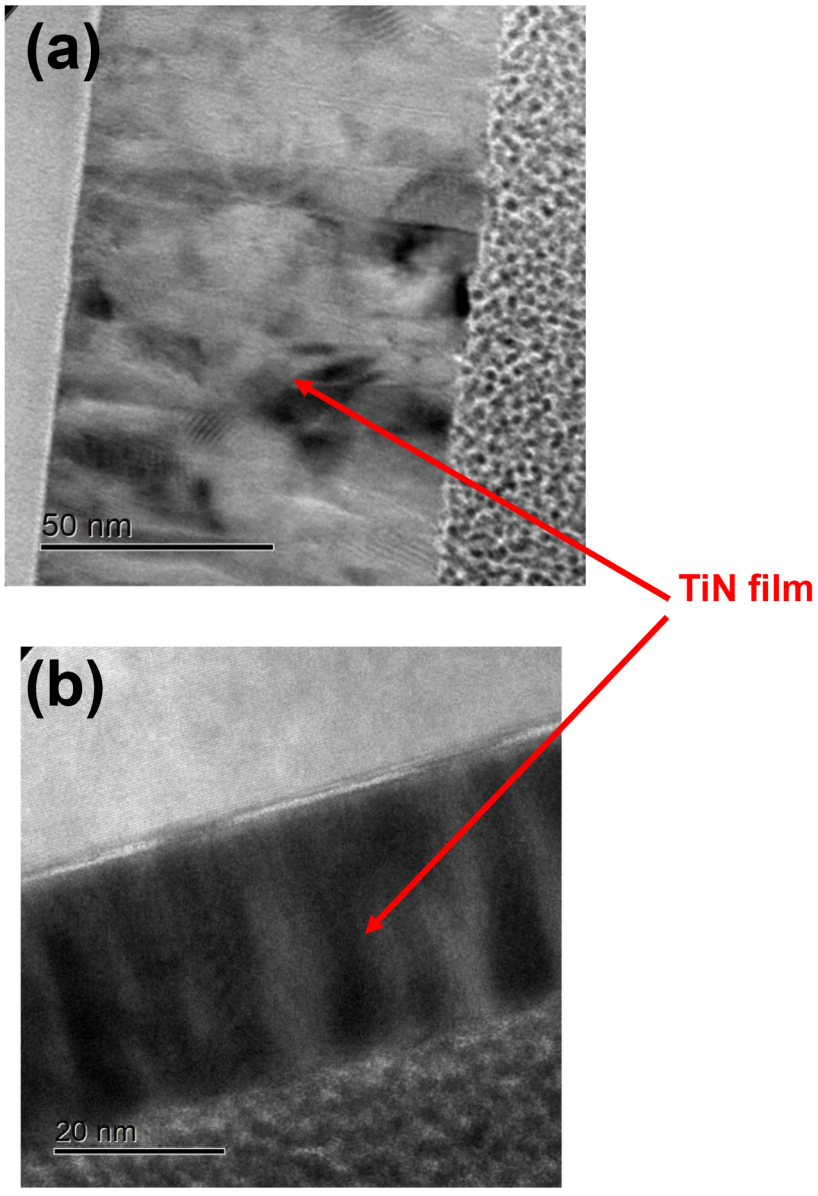

Fig. 6. High resolution transmission microscopy (HRTEM) images of TiN films grown on silicon substrate (a) film grown using sputter deposition system; (b) ALD (Atomic layer deposition) deposited film; the existence of crystalline structure is evident in both the images.

Optical Materials EXPRESS

In Table 3, we compare the optical absorption properties of 5 nm thick NbN, NbTiN, MoSi and TiN films grown by sputtering and ALD at three different wavelengths. It can be inferred from Table 3 and the data represented in Figs. 1, 3 and 4 that for MoSi films the presence of a silicon capping layer improves the extinction coefficient for the films. As discussed in [8], this enhancement may be explained by the fact that silicon is working as an additional absorbing layer below 1.1 μm. The sputter-deposited TiN film demonstrates a much higher extinction coefficient in comparison to the other two polycrystalline refractory metal-based nitride materials under consideration (NbN and NbTiN). For 2000 nm wavelength, sputtered TiN thin film has a κ value 1.36 times higher than that of NbN and 1.23 higher than that of NbTiN. For $\lambda > 1250$ nm the optical absorption of sputtered TiN film is comparable to amorphous MoSi films. At 1550 nm the TiN film shows a κ value of 4.48 while MoSi films have a κ of 4.77 and 4.88 depending on the presence of silicon cap. At the same wavelength, the optical absorption coefficient (α) of these films varies by 0.038 nm^{-1} ± 0.002 nm^{-1}. On the other hand, the ALD deposited TiN film shows a much lower value of α (0.021 nm^{-1} at 1550 nm). Hence, it can be inferred that among all the materials we have investigated in this study, sputtered TiN and amorphous MoSi thin films may serve the purpose of the most optically absorbing materials for SNSPD devices at infrared wavelengths.

Table 3. Optical absorption of 5 nm thick NbN, NbTiN, MoSi and TiN

	NbN		NbTiN		MoSi (without Si Cap)		MoSi (with Si cap)		TiN (sputtered)		TiN (ALD)	
	α (nm^{-1})	k	α (nm^{-1})	k	α (nm^{-1})	k	α (nm^{-1})	k	α (nm^{-1})	k	α (nm^{-1})	k
1000 nm	0.04	3.16	0.042	3.37	0.051	4.14	0.053	4.25	0.041	3.28	0.03	2.39
1550 nm	0.028	3.50	0.031	3.84	0.039	4.77	0.04	4.88	0.036	4.48	0.021	2.58
2000 nm	0.023	3.81	0.026	4.19	0.033	5.24	0.034	5.37	0.032	5.17	0.015	2.43

The performance of a surface plasmon polariton (SPP) in the interface of a semi-infinite metal/dielectric can be evaluated based on the propagation length (defined as the 1/e field-decay length along the direction of propagation) and the confinement width (evanescent decay length of the fields perpendicular to the interface). As discussed by [48], one important requirement for the generation of surface plasmons is real part of permittivity of the metal thin films has to be negative. (In a recent study, Giovampaola *et al.* explored the possibility of designing plasmonic nanostructures with the materials which have real part of permittivity positive [49].) If we analyse the optical constants measured in this report, it can be seen that TiN thin films grown in the sputter system have negative Re(ε) for $\lambda > 600$ nm. For the ALD grown TiN films Re(ε) changes with film thickness (shown in Fig. 7(b)). For the thinner films Re(ε) becomes more positive: for 3 nm thick film it becomes completely positive over the whole spectral range. From Fig. 7(a) it is evident that MoSi has a negative value of Re(ε) for $\lambda < 680$ nm and NbTiN shows a negative Re(ε) for the wavelength range of 490 nm to 1220 nm. At the same time, NbN retains a positive value of Re(ε) over the whole measurement range.

Optical Materials EXPRESS

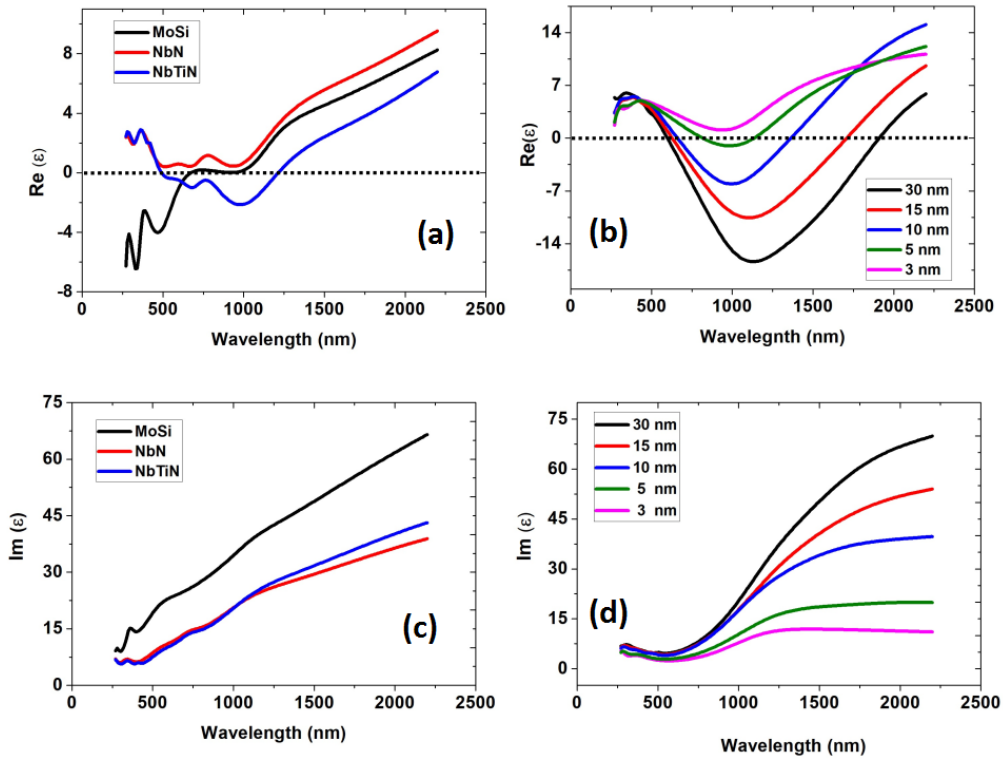

Fig. 7. Wavelength dependence of real part and imaginary part of permittivity, ε (a) Re(ε) of 5 nm thick MoSi (without any silicon cap), NbN and NbTiN thin films as a function of wavelength; (b) spectral variation of Re(ε) for TiN thin films grown in the atomic layer deposition system, thickness varying from 3 nm to 30 nm; (c) Im(ε) of 5 nm thick MoSi (without any silicon cap), NbN and NbTiN thin films; (d) Im(ε) of ALD deposited TiN films.

In Figs. 8 and 9 we compare the propagation length and beam confinement for all the thin film samples we have studied in this report for a SPP propagating in a metal/air interface. The propagation length is defined by

$$L = [2\,\mathrm{Im}(\beta)]^{-1} \tag{1}$$

where

$$\beta = \frac{2\pi}{\lambda}\sqrt{\frac{\varepsilon_m}{\varepsilon_m + 1}}; \tag{2}$$

λ denotes the excitation wavelength and ε_m is the complex permittivity of the metal. To calculate the confinement of the SPP wave at the interface we have followed the expression provided by Maier *et al*. in [48]:

$$\hat{z} = \frac{1}{|k_z|} \tag{3}$$

where

$$k_z = \sqrt{\beta^2 - (\frac{2\pi}{\lambda})^2}. \tag{4}$$

Optical Materials EXPRESS

This parameter ($\hat{z}$) quantifies the confinement of fields of the SPP waves perpendicular to the interface. From Figs. 8 and 9, it can be seen that both propagation length and field confinement follow a similar pattern of spectral variation. A smaller value of $\hat{z}$ (higher field confinement at the waveguide interface) also corresponds to smaller propagation length due to increased damping. For TiN thin films grown in the sputter deposition system, $L(\lambda)$ vary depending on film thickness. This variation is more prominent toward longer wavelengths. At 2000 nm wavelength the propagation length varies from 14 µm to 18.42 µm. For the ALD-grown TiN films, $L(\lambda)$ consistently decreases with film thickness. In Figs. 8(c) and 9(c) we compare the propagation length and confinement parameter of 5 nm thick NbN, NbTiN, MoSi and TiN films. It can be inferred from there that, MoSi has the highest propagation length (though accompanied with lowest beam confinement). NbN, NbTiN and sputtered TiN thin films demonstrate similar values of L and $\hat{z}$ (variation within 0.3 µm) at 1550 nm wavelength. At 2000 nm wavelength, their L and $\hat{z}$ values differ by ± 0.5 µm and ± 0.08 µm respectively, though, as stated earlier, at those wavelengths both NbN and NbTiN possess a positive value of Re(ε). The ALD grown TiN thin films have much smaller value of L and $\hat{z}$ comparison to other materials (5 nm thick film has a L value of 2.55 µm and $\hat{z}$ value of 0.51 µm respectively at 1000 nm wavelength). In [50], Patsalas *et al.* reports plasmonic resonance demonstrated by NbN in near ultraviolet wavelength range. The absence of plasmonic properties in NbN thin films grown in our sputter deposition system can be explained by chemical composition and structural properties which may not be favorable for plasmonic behaviour. We note that silicon substrates have been used in this study, and so lattice mismatch may have had a negative impact on the film microstructures which would in turn influence plasmonic properties of the film.

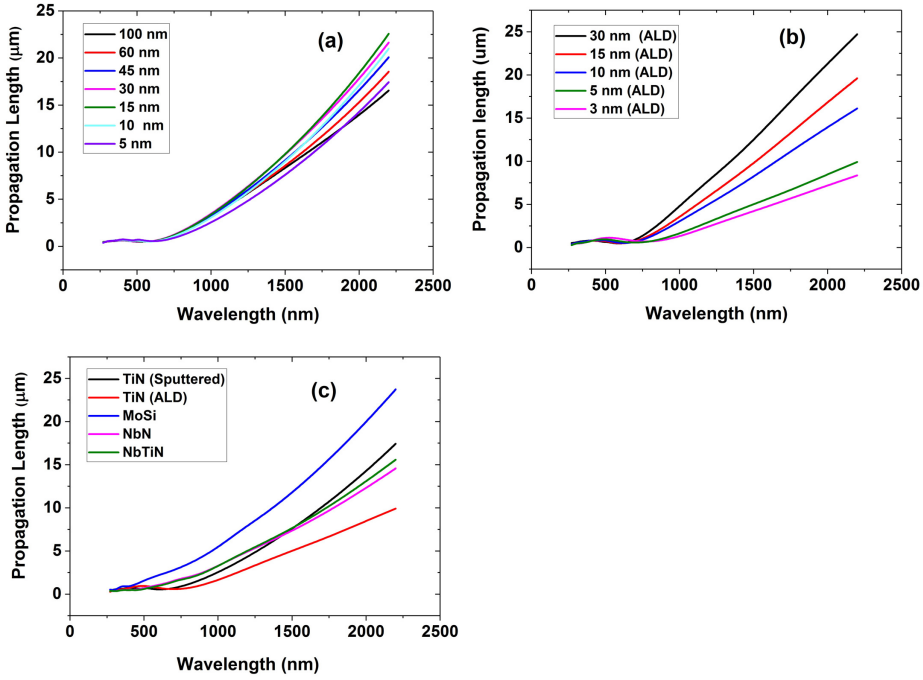

Fig. 8. Wavelength dependence of propagation length (quantifying the 1/e field-decay length along the direction of propagation of surface plasmon polariton wave in a metal/dielectric interface) of refractory metal-based thin materials we have explored in this study:(a) TiN grown in the sputter system; (b) TiN films deposited in ALD; (c) a comparison of propagation length of 5 nm thick MoSi (without Si cap), NbN, NbTiN and TiN grown by the two different techniques.

Optical Materials EXPRESS

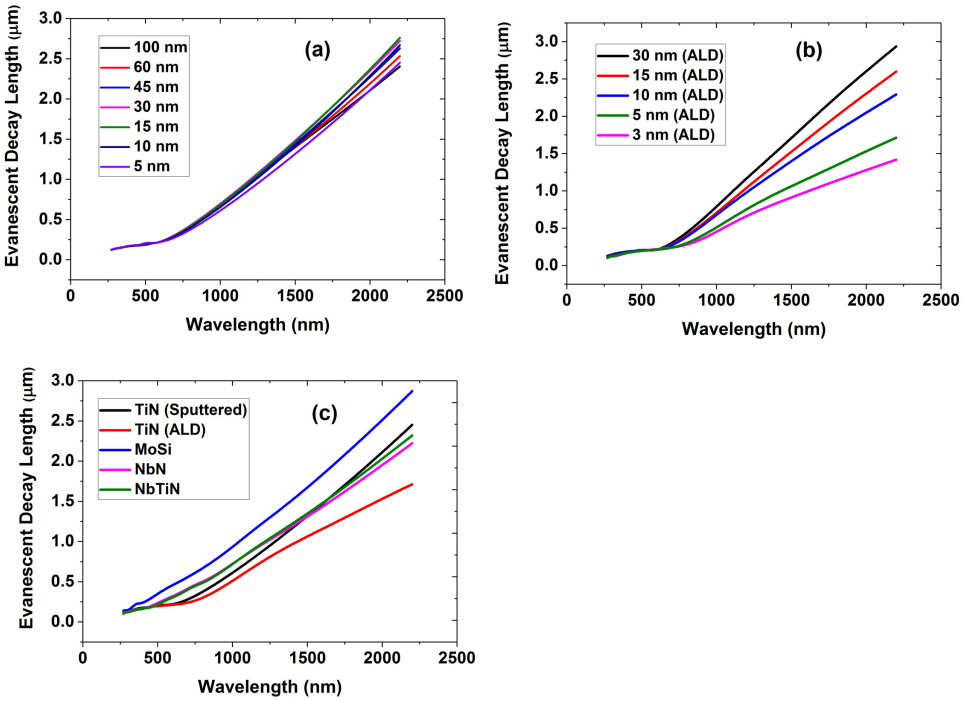

Fig. 9. Spectral variation of evanescent decay length (quantifying the confinement of surface plasmon polariton wave in a metal/dielectric interface) of refractory metal-based thin materials we have explored in this study (a) TiN grown in the sputter system; (b) TiN films deposited in ALD; (c) a comparison of propagation length of 5 nm thick MoSi (without any Si cap), NbN, NbTiN and TiN grown in the 2 different techniques.

Optical and plasmonic properties of TiN thin films grown on silicon substrates have been explored in previously reported studies [51,52]. Van Bui *et. al.* studied TiN films grown by atomic layer deposition technique (254 nm – 1688 nm wavelength range) [50]. Sputter deposited TiN films have been explored by Zgrbaik *et. al.* (500 nm – 1600 nm wavelength range) [51]. We present measurement of optical properties over a substantially longer wavelength range (270 nm –2200 nm) in comparison to the measurements carried out in these studies. The ALD-grown TiN films reported here show a completely different trend in how optical properties vary with wavelength in comparison to those reported by Bui *et. al.* However, like the measurements reported here, their results also indicate the existence of plasmonic properties (negative value of Re(ε)) in near-infrared wavelengths. A comparison of our sputtered TiN films with those reported by Zgrbaik *et. al.* shows that optical properties measured by our films follow similar trends as reported in their study (i.e. room temperature grown TiN films on silicon substrates have an intermediate composition between metallic and dielectric TiN). At 1550 nm wavelength, they report a Re(ε) value of ~-17 which is similar to the values measured from our sputtered TiN films. Bui *et. al.* also explored the correlation between film thickness and optical properties for ALD grown TiN films [51]. According to data presented by them, below 5 nm, the optical constants change rapidly with decreasing film thickness. However, the dielectric functions remain almost constant for the TiN films thicker than 7 nm. Conversely, for our films dielectric functions change gradually with film thickness over the whole measurement range. In [53], Shah *et. al.* presented a thickness dependent study of sputtered TiN thin films (thickness 2-10 nm on MgO substrate). Their films show highly metallic nature with a high negative value of Re(ε) and a decreasing trend of Re(ε) with thickness, (the 10 nm thick TiN film grown in our system shows a Re(ε) value

Optical Materials EXPRESS

of −13.42 which is ~0.24 times the value reported by their measurement and thickness dependence of Re(ε) does not follow any such trends). As explained by [52], this is due to the lattice mismatched but commonly employed substrates we chose for this study.

As discussed in Section 1, the superconducting properties of thin films show different trends with thickness which may impact their potential performance as SNSPDs. Figure 10 shows how T_c of NbTiN, MoSi and TiN deposited following the optimized growth recipes in our deposition systems varies with film thickness (room temperature deposited on silicon substrates). It can be seen that NbTiN has the highest T_c in thin film form (for a 10 nm thick film it has a T_c of 11.8 K whereas a 5 nm thick film possess T_c of 7.2 K). 5 nm thick amorphous MoSi film has a T_c of 5.5 K hence this can be a suitable amorphous material for superconducting detectors which can be operated at temperature > 2 K. As expected, TiN thin films show the weakest superconducting properties among the set of materials we have studied. Sputtered TiN films with 100 nm thickness shows a T_c of 3.4 K, and 10 nm thick films have a T_c of 1.9 K. On the other hand, for the ALD deposited TiN films the 5nm thick film has 0.67 K T_c and the 30 nm thick film shows a T_c of 2.09 K. By considering these optical, structural and superconducting properties, an appropriate material can be chosen for a given application: MoSi appears to be ideal for devices operated at temperatures > 2 K, and TiN thin films appear promising as superconducting detectors which operate beyond 2 μm, or for integration of plasmonic nanostructure and SNSPD devices.

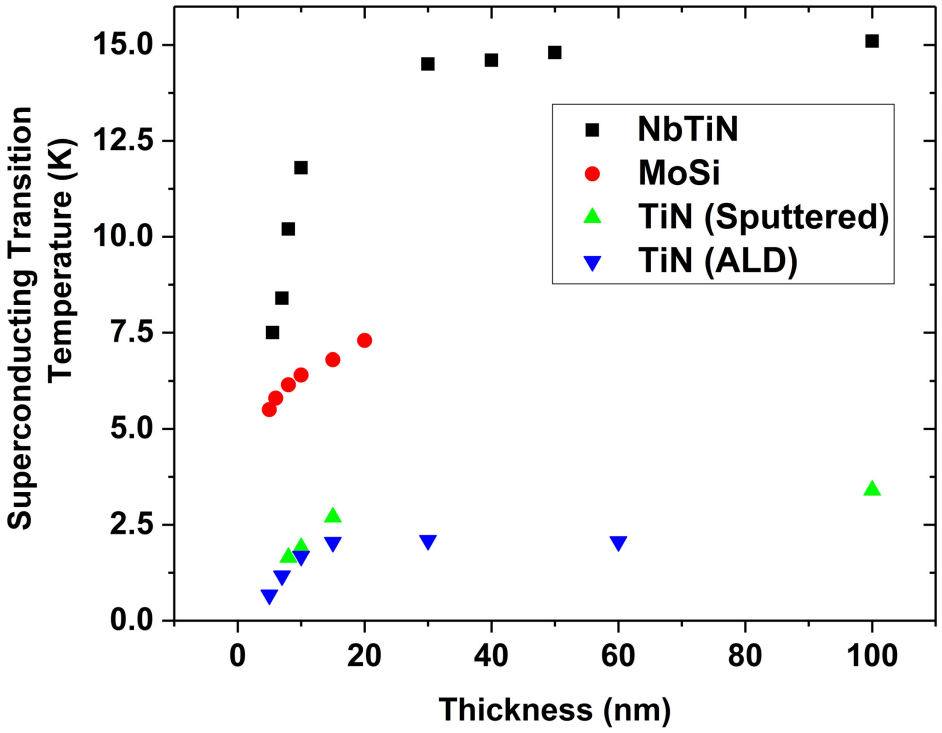

Fig. 10. Variation of superconducting transition temperature of NbTiN, MoSi and TiN (sputtered and ALD grown) films with film thickness. As described in Section 2, sputtered films have been grown on silicon substrates at room temperature and ALD TiN films were grown on silicon substrates at 350°C.

Optical Materials EXPRESS

4. Conclusion and discussion

In this report, we have explored optical properties of a selection of refractory metal based compounds and alloys for potential applications in plasmonic devices and superconductor based single photon detectors. In our study, sputter deposition was carried out at room temperature on silicon substrates. Alongside this we also studied TiN deposited via atomic layer deposition (ALD). Variable angle spectroscopic ellipsometry (VASE) was employed to measure the optical properties of the materials. In terms of optical absorption, amorphous MoSi and sputtered polycrystalline TiN films show the most efficient properties at infrared wavelength. At 1550 nm wavelength, 5 nm thick MoSi (without any Si capping layer) and TiN thin films demonstrate optical absorption coefficient of 0.039 nm^{-1} and 0.036 nm^{-1} respectively. Structural properties of thin films materials were explored with high resolution transmission electron microscopy (HRTEM). This study of optical properties enables us to control film properties, choose suitable base material for superconducting nanowire single photon detectors and design superconducting detectors for specific photon counting applications maximizing efficiency through integration with optical cavities, nanoantennas and waveguides. The materials studied have high melting points and could potentially be used in sensing and thermometry applications in harsh environments. To explore possible applications in plasmonic structures, we have studied the propagation length and confinement of surface plasmon polariton in semi-infinite air/metal interface for the thin films materials. According to the criteria of plasmonic materials, real part of electrical permittivity of the metal has to be negative [48]: sputter-deposited TiN meets this requirement for wavelengths greater than 600 nm, while MoSi follows this for $\lambda < 680$ nm. At 650 nm, it shows a 4.3 times higher L value than that of sputtered TiN film. Since MoSi has a negative value of Re(ε) in the near ultra-violet (UV) wavelength range it can be a potential plasmonic material for near UV applications [54]. NbTiN meets the condition of a plasmonic material for wavelengths from 490 nm to 1220 nm. Hence, NbTiN or MoSi can be suitable refractory metal-based alternative of TiN for high temperature plasmonic devices (MoSi in the near ultra-violet to visible and NbTiN in the visible to near infrared range).

Funding

UK Engineering and Physical Sciences Research Council (awards: EP/M01326X/1 QuantIC Quantum Technology Hub; EP/L024020/1); European Research Council Consolidator Grant (IRIS 648604).

Acknowledgments

AB thanks Plassys Bestek (France) for expert support on UHV sputtering. DH and IT thank Oxford Instruments Plasma Technology for support and shared expertise. The authors thank the technical staff of the James Watt Nanofabrication Centre (JWNC) and Kelvin Nanocharacterization Centre (KNC) at the University of Glasgow for expert support. The authors thank Dr Vincenzo Giannini (Imperial College, London) for valuable feedback on this study.